arXiv:1101.2526v1 [gr-qc] 13 Jan 2011

Tuning Time-Domain Pseudospectral Computations of the Self-Force on a Charged Scalar Particle

Priscilla Canizares and Carlos F. Sopuerta

Institut de Ciències de l'Espai (CSIC-IEEC), Facultat de Ciències, Campus UAB, Torre C5 parells, Bellaterra, 08193 Barcelona, Spain

E-mail: pcm@ieec.uab.es, sopuerta@ieec.uab.es

Abstract. The computation of the self-force constitutes one of the main challenges for the construction of precise theoretical waveform templates in order to detect and analyze extreme-mass-ratio inspirals with the future space-based gravitational-wave observatory LISA. Since the number of templates required is quite high, it is important to develop fast algorithms both for the computation of the self-force and the production of waveforms. In this article we show how to tune a recent time-domain technique for the computation of the self-force, what we call the Particle without Particle scheme, in order to make it very precise and at the same time very efficient. We also extend this technique in order to allow for highly eccentric orbits.

PACS numbers: 04.20.-q,04.25.Nx,04.30.Db,02.70.Hm

AMS classification scheme numbers: 35Q75,65M70,83C10

Submitted to: *Class. Quantum Grav.*

1. Introduction

Gravitational Wave Astronomy has the potential to unveil the secrets of physical phenomena not yet understood involving strong gravitational fields. In order to realize this potential there are observatories/detectors either operating or being design/constructed that cover a significant part of the relevant gravitational-wave frequency spectrum. From the very low band ($10^{-9} - 10^{-6}$ Hz), where we have the pulsar timing arrays to the high frequency band ($1 - 10^4$ Hz), where most ground-based detectors operate. In low frequency band ($10^{-4} - 1$ Hz), not accessible from the ground, we find the future Laser Interferometer Space Antenna (LISA) [1], an ESA-NASA mission consisting of three spacecrafts forming a triangular constelations in heliocentric orbit (see [2, 3] for details). The targets of LISA are: (i) massive black hole (BH) mergers; (ii) the capture and subsequent inspiral of stellar compact objects (SCO) into a massive BH sitting at a galactic center; (iii) galactic compact binaries; and (iv) stochastic backgrouns of diverse cosmological origin.

For many of these systems it is crucial to have a priori gravitational waveform models with enough precision to extract the corresponding signals from the future LISA data stream, and also to estimate the physical parameters of the system with precision. Here we focus in the second type of LISA sources, namely the so-called extreme-mass-ratio inspirals (EMRIs). The EMRIs of interest for LISA consists of massive BHs with masses in the range $M = 10^4 - 10^7 M_\odot$, and SCOs with masses in the range $m = 1 - 50 M_\odot$. The SCO moves around the massive BH following highly relativistic motion well inside the strongest field region of the BH. The orbit is not exactly a geodesic of the BH because of the SCO own gravity, which influences its own motion, making the orbit to shrink until it plunges into the BH. During the last year before plunge, it has been estimated [4] that the SCO spends of the order of 10^5 cycles (depending on the type of orbit) inside the LISA band. As a consequence the EMRI GWs carry a detailed map of the BH geometry. This will allow, in particular, to test the spacetime geometry of BHs and even alternative theories of gravity (see, e.g. [5, 6, 7]). We can also understand better the stellar dynamics near galactic nuclei, populations of stellar BHs, etc. (for a review see [8]).

All this requires very precise EMRI gravitational waveforms (the precision of the phase should be of the order of one radian per year). Due to the extreme mass ratio of these systems, $\mu = m/M \sim 10^{-7} - 10^{-3}$, we can describe them in the framework of BH perturbation theory, where the SCO is modeled as a point-like mass and the backreaction effects are described as the effect of a local force, the so-called *self-force*. This self-force is essentially determined by the derivatives of the metric perturbations (retarded field) at the particle location, which need to be regularized due to the singularities introduced by the particle description. The calculation of the retarded field has to be done numerically, either in the frequency or time domain. In this work we concentrate on a recent approach to self-force calculations in the time domain introduced in [9, 10] for circular orbits and extended to eccentric orbits in [11]. This is a multidomain approach in which the point particle is always located at a node between two domains, and hence it has been named the Particle without Particle (PwP) scheme. The main advantage is that the equations to be solved are homogeneous and the particle location enters via junction/matching conditions. In this way we are dealing with smooth solutions at each domain, which is crucial for the convergence of the numerical method used to implement the method, the PseudoSpectral Collocation (PSC) method in our case.

In this article we describe how to tune the numerical implementation of the PwP scheme to achieve high precision results with modest computational resources. We focus on two fronts: (i) How to change the framework introduced in [10, 11] to compute the self-force for orbits with high eccentricity, and (ii) how to pick the size of the computational domain in order to make our computations much more efficient, so that we can achieve very precise results with a modest amount of computational resources. A similar analysis for a different computational technique has been presented in [12].

The plan of the paper is the following: In Sec. 2 we describe briefly the foundations of self-force calculations in a simplified model based on a charged particle orbiting a non-rotating BH. In Sec. 3 we summarize the PwP scheme and extend the multidomain structure in order to allow for computations in the case of high eccentric orbits. We also show the convergence properties of the PSC method numerical implementation. In Sec. 4 we describe how to choose the resolution depending on the mode in order to perform optimal calculations in the sense of computational resources. We finish with conclusions and a discussion in Sec. 5, where we also present some numerical results.

2. Scalar charged particle orbiting a non-rotating BH

The dynamics of a scalar charged particle is governed by the equation of motion of the associated scalar field (see, e.g. [13]):

$$\mathrm{g}^{\alpha\beta}\nabla_\alpha\nabla_\beta\Phi(x) = -4\pi q\int_\gamma d\tau\,\delta_4(x,z(\tau))\,, \tag{1}$$

and its own equation of motion

$$m\,\frac{du^\mu}{d\tau} = F^\mu = q\,(\mathrm{g}^{\mu\nu}+u^\mu u^\nu)\,(\nabla_\nu\Phi)|_\gamma\ , \quad u^\mu = \frac{dz^\mu}{d\tau}\,. \tag{2}$$

where m, q, and γ are the particle mass, charge, and timelike worldline (parameterized as $x^\mu = z^\mu(\tau)$, being τ proper time) respectively, $\mathrm{g}^{\alpha\beta}$ is the spacetime inverse metric (the BH metric, the Schwarzschild metric in our case), ∇_μ the associated canonical connection, and $\delta_4(x,x')$ is the invariant Dirac delta distribution. These two equations are coupled [Eq. (1) is a partial differential equation whereas Eq. (2) is an ordinary differential equation]. Eq. (1) describes the retarded scalar field generated by the particle and Eq. (2) how this field affects in turn the particle trajectory, mimicking the backreaction mechanism that produces the inspiral of EMRIs in the gravitational case (see [14, 13] for reviews on the self-force problem).

Since we are dealing with a non-rotating BH, using the spherical symmetry we can expand the retarded field in scalar spherical harmonics

$$\Phi(x^\mu) = \sum_{\ell=0}^{\infty}\sum_{m=-\ell}^{\ell}\Phi^{\ell m}(t,r)Y^{\ell m}(\theta,\varphi)\,, \tag{3}$$

so that each harmonic mode $\Phi^{\ell m}(t,r)$ satisfies a $1+1$ wave-type equation:

$$\left\{-\frac{\partial^2}{\partial t^2}+\frac{\partial^2}{\partial r^{*2}}-V_\ell(r)\right\}(r\,\Phi^{\ell m}) = S^{\ell m}\delta(r-r_{_p}(t))\,, \tag{4}$$

where $r_{_p}(t)$ is the radial trajectory of the particle, $r^* = r+2M\ln(r/2M-1)$ is the radial *tortoise* coordinate, M is the BH mass, and $V_\ell(r)$ is the Regge-Wheeler potential for scalar fields

$$V_\ell(r) = f(r)\left[\frac{\ell(\ell+1)}{r^2}+\frac{2M}{r^3}\right]\,, \qquad f(r) = 1-\frac{2M}{r}\,, \tag{5}$$

where $S^{\ell m}$ is the coefficient of the distributional source term due to the presence of the particle given by

$$S^{\ell m} = -\frac{4\pi q f(r_p)}{r_p u^t}\, \bar{Y}^{\ell m}\left(\frac{\pi}{2}, \varphi_p(t)\right) , \tag{6}$$

where $\varphi_p(t)$ is the azimuthal trajectory of the particle and we have assumed, without loss of generality, that the orbit takes place at the equatorial plane $\theta = \pi/2$. The singular character of this source term makes the retarded field to diverge at the particle location. Therefore, in order to obtain a meaningful self-force through Eq. (2) we must use a regularization scheme. We employ the *mode sum* regularization scheme [15, 16, 17, 18, 19, 20] (see also [21, 22]), which provides an analytical expression for the singular part of the retarded field mode by mode, $\Phi^{\ell m}_{\rm S}$, at the particle location. Hence, by subtracting this singular contribution from the full retarded field modes, $\Phi^{\ell m}$ (which are finite at the particle location), we obtain a smooth and differentiable field at the particle location, $\Phi^{\ell m}_{\rm R} = \Phi^{\ell m} - \Phi^{\ell m}_{\rm S}$. Adding all the harmonic modes we obtain the full regular field, $\Phi_{\rm R}$, from which we can obtain the scalar self-force as in Eq. (2), that is

$$F^{\mu}_{\rm SF} = q\left(g^{\mu\alpha} + u^{\mu}u^{\alpha}\right)\left(\nabla_{\alpha}\Phi_{\rm R}\right)|_{\gamma} . \tag{7}$$

3. Formulation of the PwP scheme

From the previous discussion it is clear that the main challenge is the computation of the harmonic modes of the retarded scalar field. This has to be done numerically and here we describe the scheme and numerical implementation that we use. We solve Eq. (4) in the time domain. To that end we use a multi-domain framework in which the particle is located always at a node in the interface between two domains, what we call the PwP scheme. The main advantage of the PwP scheme is that it avoids the presence of the singularity associated with the particle in the scalar field equations, which is crucial for the convergence properties of the numerical method. The particle then enters as junction conditions of the different domains. This idea was already used in [23] for the computation of energy and angular momentum fluxes for all kinds of orbits. The scheme was used for the computation of the self-force for the first time in [10] for the circular case, and extended in [11] to the eccentric case. Nevertheless, the scheme as presented in [11] can be used for moderate eccentricities, typically $e \lesssim 0.5$. The reason for this is that in the eccentric case the one-dimensional spatial grid needs to be changed in time in order to keep the particle at a boundary node. In [11] only the domains adjacent to the particle change in time, which limits the eccentricity of the orbits. This limitation is related to the turning points of the orbital motion (pericenter and apocenter), where one of the domains is effectively much larger than the other. In the large domain the resolution will be poor for high eccentricities, whereas in the small domain it will be high but this imposes a very restrictive Courant-Friedrichs-Lax (CFL) condition on the time step, specially in the case of PSC methods, where the CFL condition is proportional to $1/N^2$, being N the number of collocation points per domain. Therefore, pushing the scheme as it is for high eccentricities means to increase dramatically the computational resources required to obtain precise estimations of the self-force.

Here we reformulate the PwP to allow for such high eccentricity orbits, which are of interest for the EMRIs that LISA is expected to observe (see, e.g. [8]). The one-dimensional spatial domain $r^* \in (-\infty, +\infty)$ is truncated from both sides, so that the

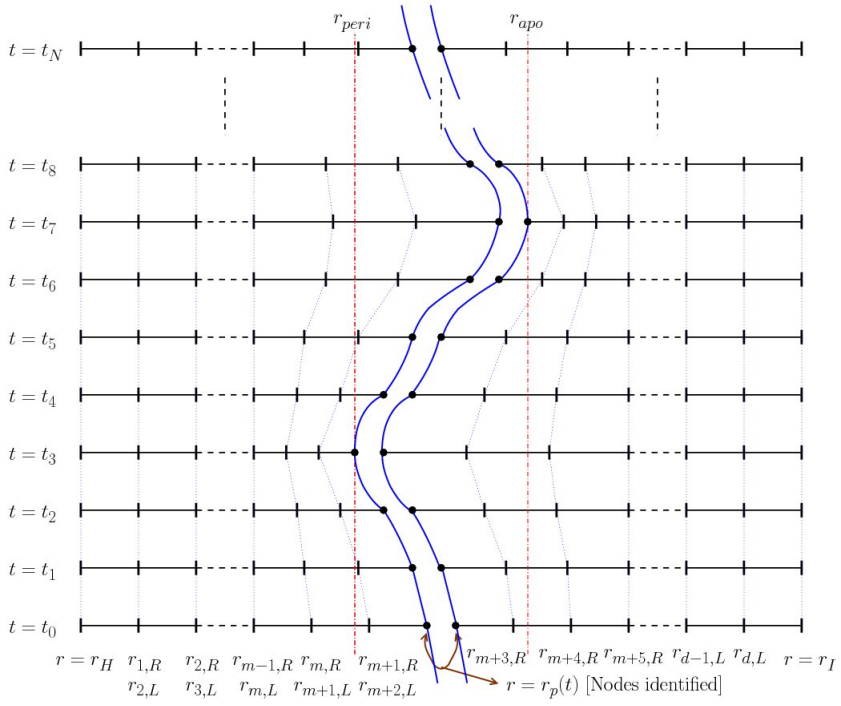


Figure 1. Structure of the one-dimensional spatial computational domain for a generic orbit. The trajectory is bounded to the interval between the pericenter (r_{peri}) and the apocenter (r_{apo}). In the setup shown there are three dynamical domains to the left and right of the particle, namely $[r^*_{m,\mathrm{L}}, r^*_{m,\mathrm{R}}] \cup [r^*_{m+1,\mathrm{L}}, r^*_{m+1,\mathrm{R}}] \cup [r^*_{m+2,\mathrm{L}}, r^*_{m+2,\mathrm{R}}]$ (left) and $[r^*_{m+3,\mathrm{L}}, r^*_{m+3,\mathrm{R}}] \cup [r^*_{m+4,\mathrm{L}}, r^*_{m+4,\mathrm{R}}] \cup [r^*_{m+5,\mathrm{L}}, r^*_{m+5,\mathrm{R}}]$ (right) with $r^*_{m+2,\mathrm{R}} = r^*_{m+3,\mathrm{L}} = r^*_p$. The figure illustrates how the dynamical domains change their coordinate size to adapt to the particle motion.

global computation domain is $\Omega = [r^*_{\mathrm{H}}, r^*_{\mathrm{I}}]$, where r^*_{H} corresponds to the truncation in the direction to the BH horizon and r^*_{I} corresponds to the truncation in the direction to spatial infinity. Now, we divide Ω in a set of subdomains: $\Omega = \cup_{a=1}^{d} \Omega_a$, where $\Omega_a = \left[r^*_{a,\mathrm{L}}, r^*_{a,\mathrm{R}}\right]$ with $r^*_{a,\mathrm{R}} = r^*_{a+1,\mathrm{L}}$ $(a = 1, \ldots, d-1)$. We consider two types of domains, *static* ($\dot{r}^*_{a,\mathrm{L}} = \dot{r}^*_{a,\mathrm{R}} = 0$) and *dynamic* (either $\dot{r}^*_{a,\mathrm{L}} \neq 0$ or $\dot{r}^*_{a,\mathrm{R}} \neq 0$). For instance, the domains surrounding the particle, $\Omega_{\mathrm{P}-1} = \left[r^*_{\mathrm{P\text{-}1,L}}, r^*_p\right]$ and $\Omega_{\mathrm{P}} = \left[r^*_p, r^*_{\mathrm{P,R}}\right]$ (where P is the number of the domain with the particle at the left node, Ω_{P}, and hence $r^*_{\mathrm{P\text{-}1,R}} = r^*_{\mathrm{P,L}} = r^*_p$), are dynamical. Then, generalizing the setup presented in [11], here we consider an arbitrary number of dynamical domains. Those domains are all around the particle as shown in Figure 1. In the case of circular orbits ($r_p(t) = const.$) all domains are static.

We discretize the spatial domain using the PSC method (see, e.g. [24]). For this purpose, each physical domain Ω_a $(a = 1, \ldots, d)$ is associated with a *spectral* domain, $[-1, 1]$ as we use Chebyshev polynomials as the basis functions for the spectral expansions, which is discretized independently. Our choice of discretization is the *Lobatto-Chebyshev* grid, with collocation points given by $X_i = -\cos(\pi\, i\,/\,N)$ $(i = 0, \ldots, N)$. Of course, the physical and spatial domains have to be mapped and

this is the crucial point for our numerical implementation of the PwP scheme. For a given domain $\Omega_a = \left[r^*_{a,\mathrm{L}}, r^*_{a,\mathrm{R}}\right]$ $(a = 1, \ldots, d)$, the spacetime mapping to the spectral domain is taken to be linear

$$\begin{array}{rccc} X_a & : & \mathbb{T} \times \left[r^*_{a,\mathrm{L}}, r^*_{a,\mathrm{R}}\right] & \longrightarrow & \mathbb{T} \times [-1,1] \\ & & (t, r^*) & \longmapsto & (T, X_a) \end{array} \tag{8}$$

where $\mathbb{T} = [t_{ini}, t_{end}]$ is the evolution time interval and

$$T(t) = t\,, \qquad X_a(t, r^*) = \frac{2r^* - r^*_{a,\mathrm{L}} - r^*_{a,\mathrm{R}}}{r^*_{a,\mathrm{R}} - r^*_{a,\mathrm{L}}}\,. \tag{9}$$

The inverse (linear) mappings from the spectral domain to each of the subdomains Ω_a are given by

$$\begin{array}{rccc} r^*|_{\Omega_a} & : & \mathbb{T} \times [-1,1] & \longrightarrow & \mathbb{T} \times \left[r^*_{a,\mathrm{L}}, r^*_{a,\mathrm{R}}\right] \\ & & (T, X) & \longmapsto & (t, r^*) \end{array} \tag{10}$$

where

$$t(T) = T\,, \qquad r^*(T,X)|_{\Omega_a} = \frac{r^*_{a,\mathrm{R}} - r^*_{a,\mathrm{L}}}{2} X + \frac{r^*_{a,\mathrm{L}} + r^*_{a,\mathrm{R}}}{2}\,. \tag{11}$$

The only thing left is to prescribe the time evolution of the boundary nodes of the dynamical domains. When there are only two dynamical domains, as in [11], the evolution of their nodes is quite simple as shown above: $r^*_{\text{P-1,L}} = const.$, $r^*_{\mathrm{P,R}} = const.$, and $r^*_{\text{P-1,R}} = r^*_{\mathrm{P,L}} = r^*_p(t)$. Now, let us consider the situation where we have N_d dynamical domains at each side of the particle, $2N_d$ in total (Figure 1 shows the case $N_d = 3$). Following Figure 1, let us assume that the first dynamical domain is $\Omega_m = [r^*_{m,\mathrm{L}}, r^*_{m,\mathrm{R}}]$, which means that $\mathrm{P} = m + N_d$, that is

$$\begin{aligned} \Omega = {} & [r^*_{\mathrm{H}}, r^*_{1,\mathrm{R}}] \cup \cdots \cup [r^*_{m,\mathrm{L}}, r^*_{m,\mathrm{R}}] \cup \cdots \cup [r^*_{m+N_d-1,\mathrm{L}}, r^*_p] \cup [r^*_p, r^*_{\mathrm{P,R}}] \\ & \cup \cdots \cup [r^*_{\mathrm{P}+N_d-1,\mathrm{L}}, r^*_{\mathrm{P}+N_d-1,\mathrm{R}}] \cup \cdots \cup [r^*_{d,\mathrm{L}}, r^*_{\mathrm{I}}]\,. \end{aligned} \tag{12}$$

The criterium that we use to determine the motion of the dynamical domains is to demand that all of them to the left of the particle have the same coordinate size (in terms of the radial tortoise coordinate) at any given time, and the same for those to the right of the particle. This completely determines the evolution of the dynamical domains. Then, the motion of the dynamical nodes to the left of the particle is described by the following equations $(a = m, \ldots, m + N_d - 1)$:

$$r^*_{a,\mathrm{L}} = r^*_{m,\mathrm{L}} + (a - m)\frac{r^*_p - r^*_{m,\mathrm{L}}}{N_d}\,, \tag{13}$$

$$r^*_{a,\mathrm{R}} = r^*_{m,\mathrm{L}} + (a - m + 1)\frac{r^*_p - r^*_{m,\mathrm{L}}}{N_d}\,, \tag{14}$$

and the motion of the ones to the right of the particle by $(a = \mathrm{P}, \ldots, \mathrm{P} + N_d - 1)$

$$r^*_{a,\mathrm{L}} = r^*_p + (a - \mathrm{P})\frac{r^*_{\mathrm{P}+N_d-1,\mathrm{R}} - r^*_p}{N_d}\,, \tag{15}$$

$$r^*_{a,\mathrm{R}} = r^*_p + (a - \mathrm{P} + 1)\frac{r^*_{\mathrm{P}+N_d-1,\mathrm{R}} - r^*_p}{N_d}\,, \tag{16}$$

where $r^*_{m,\mathrm{L}}$ and $r^*_{\mathrm{P}+N_d-1,\mathrm{R}}$ are the fixed boundary nodes that separate the static from the dynamical domains. The r^*-coordinate size of the dynamical domains changes according to the motion of the particle, as illustrated in Figure 1.

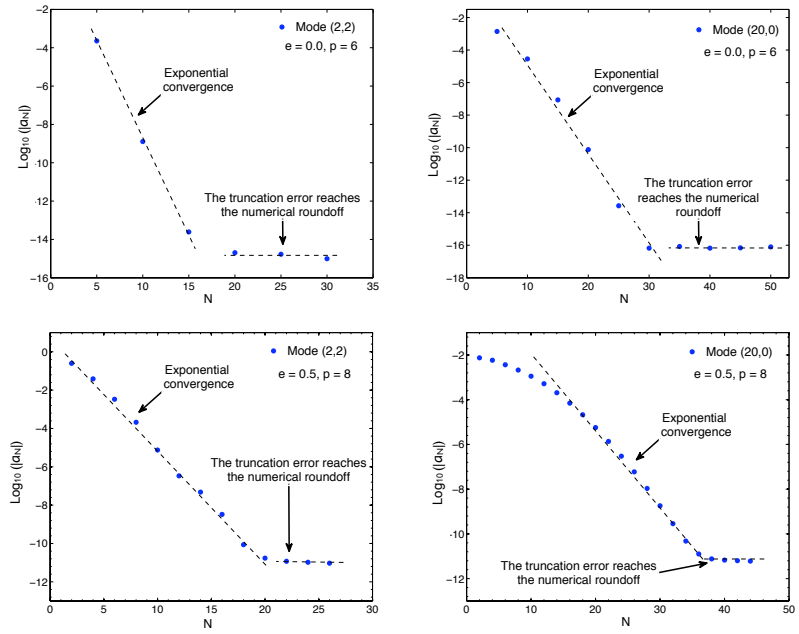


Figure 2. Convergence plots ($\log_{10}|a_N|$ versus N) for the variable $\psi = r\,\Phi^{\ell m}$. The upper row corresponds to a circular orbit with $r = 6M$ (last stable orbit) and the lower row to an eccentric orbit with $(e, p) = (0.5, 8.0)$. The left column shows results for the harmonic mode $(\ell, m) = (2, 2)$ and the right column for $(\ell, m) = (20, 0)$. The data have been obtained from the domain to the right of the particle, whose coordinate size, Δr^*, is $5M$ for the circular case and in the eccentric case varies, due to the fact that the domain is dynamical, in the range $1 - 15M$. We can see how exponential convergence is achieved until machine roundoff is reached.

After discretizing the domain, we need to discretize the variables and equations. Since nothing essential changes with respect to the description given in [11], we just summarize here the main points. First we reduce the wave-type equation (4) to a first-order symmetric hyperbolic system by introducing the following variables $(\psi, \psi, \varphi) = (r\,\Phi^{\ell m}, \partial_t \psi^{\ell m}, \partial_{r^*} \psi^{\ell m})$. Then, the restriction of these variable to every single domain satisfies a set of homogeneous equations, i.e. without Dirac delta distributions. This means that at each domain we obtain smooth solutions. This is the main property of the PwP scheme and of its implementation. The fact that the solutions at each domain are smooth preserves the exponential convergence property of the PSC method. At the same time, the scheme avoids the presence of singularities and hence, the need of using implementations that introduce artificial spatial scales in the problem in order to deal with the particle. We show the convergence properties of our computations in Figure 2, where we plot an estimation of the truncation error based on the value of the last spectral coefficient, $\boldsymbol{a}_N$, with respect to the number of collocation points, N.

The other important point of the PwP scheme is the communication of the solutions from the different domains across their boundaries. This is done by using the junction conditions dictated by our field equations (see [23, 10, 11]). In the case of boundaries that do not contain the particle this translates to impose continuity of

the retarded field and its first-order time and radial derivatives. When the particle is present the junction conditions translate into jumps in the derivatives (not in the retarded field itself). The junction conditions are imposed in pratice using two different methods described in [11]: (i) The *penalty* method, and (ii) the direct communication of the characteristic fields.

For the spatial discretization of our variables, $\boldsymbol{U} = (\psi, \psi, \varphi)$, the PSC method provides two representations: (i) the *physical* one, based on the values of the variables at the collocation points, $\{\boldsymbol{U}_i\}_{i=0,\ldots,N}$; (ii) the *spectral* representation, based on the coefficients of the truncated expansion in Chebyshev polynomials, $\{\boldsymbol{a}_n\}_{n=0,\ldots,N}$. We change from one representation to the other by means of transformation matrices or, in a more efficient way, by means of fast Fourier transformations [24]. Finally, the discretization in time, the evolution algorithm, is done using a Runge-Kutta 4 algorithm.

4. Tuning the Domain Size to the Harmonic Number m

In the formulation and implementation of the PwP scheme presented in [10, 11] it was already shown that precise calculations of the self-force with modest computational resources (less than an hour in a computer with two Quad-Core Intel Xeon processors at 2.8 GHz) is possible. However, as already discussed in [10, 11], there is a room for improvement in different aspects of the numerical implementation. Here, we show how to improve what we believe is the most important aspect: the distribution of domain sizes with respect to the harmonic number m. To that end, we use a phenomenological approach to this question, restricting ourselves to the particular case of circular orbits.

The scalar field harmonic modes produced by a charged particle in circular motion are like *forced* oscillators, with a force term given by $S^{\ell m}\,\delta(r - r_p)$ [see Eq. (4)], which oscillates periodically in time. More precisely, $S^{\ell m} \propto \exp(i\,m\,\omega_p\,t)$, where $\omega_p = M^{1/2} r_p^{-3/2}$ is the particle's angular velocity. The potential V_ℓ decays quite fast away from the location of its maximum, so that the field looks like a monocromatic wave in the regions where the potential is not important. The wavelength of these waves is $\lambda_m = \lambda_1/m$, where $\lambda_1 = 2\pi/\omega_p$ is the wavelength of the $m = 1$ modes. Therefore in a domain Ω_a, with coordinate size $\Delta r^* = r^*_{a,\mathrm{R}} - r^*_{a,\mathrm{L}}$, modes with different harmonic number m require different resolutions, understood as the ratio $\Delta r^*/N$, in order to resolved them with the same accuracy. For instance, given two modes $\Phi^{\ell m}$ and $\Phi^{\ell' m'}$ such that $m < m'$, i.e. with $\lambda_m > \lambda'_m$, in a given domain Ω_a we will find more wavelengths of the mode $\Phi^{\ell' m'}$ than the mode $\Phi^{\ell m}$. This means we need more resolution for the mode $\Phi^{\ell' m'}$ than for the mode $\Phi^{\ell m}$ in order to achieve comparable accuracy.

Here, we can change Δr^* and the number of domains d (if we reduce Δr^* we need more domains and the converse), or N, or both. The question here is what is the optimum way of setting the resolution for each m-mode, in the sense of minimizing the computational resources. Increasing the resolutions means to increase the number of computer operations, and in this sense it is not the same to increase the number of domains, decreasing their size (see [10] for a discussion of this point), than to increase the number of collocation points (using FFT instead of matrices, the number of operations in the relevant part of the algorithm scales with N as $N \ln N$). In order to investigate this question we have conducted a series of simulations to study the behavior of different modes of the retarded field $\Phi^{\ell m}$ under changes of the coordinate

domain size Δr^* and the number of collocation points N. The results for values at the particle location for the modes $\Phi^{8,2}$ and $\Phi^{8,8}$ are shown in Figure 3. As we can see, it is crucial to choose carefully Δr^* for a fixed value of N, otherwise we can find ourselves in one of the following situations: Either Δr^* is too big and then, N collocation points are not enough to resolve all the modes, or Δr^* is too small and we are using too many collocation points, i.e. we are performing too many numerical computations to resolve the modes.

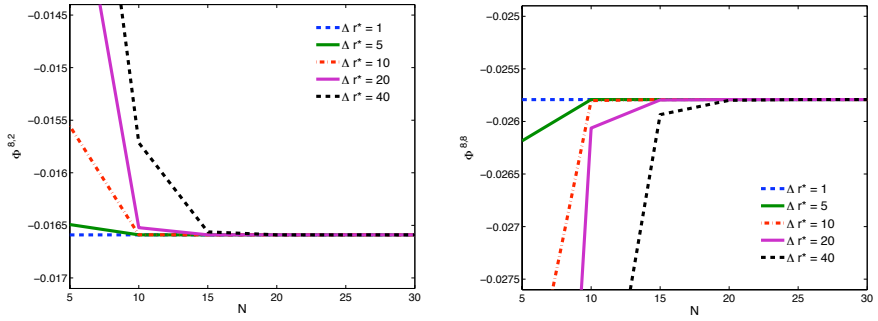


Figure 3. This figure shows values of the $\Phi^{8,2}$ (left) and $\Phi^{8,8}$ (right) modes of the retarded field at the particle location as computed from the domain to the right of it ($\Omega_{\rm P}$), with respect to the number of collocation points N. Each line correspond to a different coordinate size of the domain where the calculations are done: $\Delta r^*/M = 1, 5, 10, 20, 40$. It shows how the values of the modes converge as Δr^* is decreased and N is increased. It is remarkable to realize that for small coordinate size the convergence is reached with few collocation points.

From our simulations we have found that adjusting the size of the domains to the wavelength of the modes of the retarded field, i.e. $\Delta r^* \simeq \lambda_m$, the values of the field converge and are resolved for a minimum of collocation points given by $N \sim \Delta r^*/(2M) + 25$. This provides us with a rule of thumb for the choice of the domain size and number of collocation points as a function of m: $\Delta r^*(m) \sim \lambda_m$ and $N(m) = [\Delta r^*/(2M) + 25]$ (where here $[x]$ denotes the integer closest to x).

Another strategy that has been used in the literature (see [25, 12]) is to truncate the mode series for the self-force at a given $\ell = \ell_{\rm T}$ and then, to estimate the remaining infinite number of terms by using the known large-ℓ series [21]. The idea is to fit the coefficients of this series by least-squares fitting to a subset of the numerically estimated self-force modes (i.e. with $\ell \leq \ell_{\rm T}$). We have not used this procedure in this paper because our aim is to tune our numerical scheme, but it can certainly be used in order to complement and improve the results that we obtain.

5. Conclusions and Discussion

The PwP scheme introduced and developed in [9, 10, 11] provides a framework for precise and efficient computations of the self-force in the time domain. In this paper we have investigated how to tune the method in order to increase its efficiency and accuracy. We have also extended the PwP scheme in order to make it suitable for computations of the self-force on highly eccentric orbits.

We have studied how to distribute the domain sizes and the number of collocation points so that we allocate the optimum resolution to each harmonic mode. This is very

important as the resolution requirement increases with m, despite the fact that high ℓ-modes contribute less to the self-force than low ℓ ones. This means that in order to improve the accuracy of the self-force we must have a good control of the resolution, otherwise modes with high m (and hence with high ℓ) will limit the precision despite not contributing much to the self-force.

Using this information, we have conducted a series of computations of the self-force for the case of a scalar charged particle in circular (geodesic) orbits around a non-rotating BH. The computational parameter space that we have explored is described as follows: The total number of domains that we have used is in the range $d = 20-43$. The coordinate size of the large domains (the ones far from the particle and near the boundaries) is in the range $\Delta r^* = 50 - 100M$. The number of collocation points has been fixed to $N = 50$. The largest ℓ, $\ell_{\rm max}$, considered in the computations is in the range $\ell_{\rm max} = 20 - 40$.

Adapting the resolution for each m-mode also allows us to adapt the time step as the CFL condition is proportional to the minimum coordinate physical distance (as measured in terms of the tortoise radial coordinate) between grid points (and inversely proportional to the square of the number of collocation points). This means that the number of time steps required, N_t, for a simulation is going to be proportional to m as: $N_t^m = m\, N_t^{m=1}$. This is assuming that we use the same number of domains for all modes, but it is clear that modes with low m would need less domains than modes with high m, and therefore, this is another source of reduction of computational time.

We have been able to obtain very precise values of the self-force for a wide range of values within the parameter space. For instance, in the case of the radial component of the regular field, $\Phi_r^{\rm R}$, the only one that for the circular case needs regularization, we have obtained values like $\Phi_r^{\rm R} = 1.677282 \times 10^{-4}\, q/M^2$, which have a relative error of the order of $5 \cdot 10^{-5}\,\%$ with respect to the values obtained in [25] using frequency-domain methods. The relative error is always in the range $5\cdot 10^{-5}\,\% - 5\cdot 10^{-3}\,\%$. This constitutes a significant improvement with respect to our own previous estimations presented in [10], where the relative errors quoted for $\Phi_r^{\rm R}$ were of the order of 0.1%. The typical time for a full self-force calculation in a computer with two Quad-Core Intel Xeon processors at 2.27 GHz is in the range $10 - 15$ minutes, which is a very significant reduction with respect to our computations in [10], specially taking into account that we have also improved the precision of the self-force computations.

The calculations we have presented can be further improved in terms of computational time, and perhaps in accuracy by exploring techniques to bring the boundaries closer to the particle without degrading the accuracy of the field values near it. This can be done either by improving the outgoing boundary conditions (see, e.g. [26]) or by using some sort of compactification of the physical domain (see, e.g. [27]). Another possibility for making the computations faster (although this does not decrease the CPU time) is to parallelize the code and use computers with many cores. This is in principle a simple task as the different modes are not coupled. In any case, the next step in this line of work is to perform a similar phenomenological study for the eccentric case, where not only the azimuthal frequency is important, but also the radial one, which is absent in the circular case.

Acknowledgments

P.C.M. is supported by a predoctoral FPU fellowship of the Spanish Ministry of Science and Innovation (MICINN). C.F.S. acknowledges support from the Ramón y Cajal

Programme of the Ministry of Education and Science (MEC) of Spain, by a Marie Curie International Reintegration Grant (MIRG-CT-2007-205005/PHY) within the 7th European Community Framework Programme (EU-FP7), and contracts ESP2007-61712 (MEC) and No. FIS2008-06078-C03-01/FIS (MICINN). We acknowledge the computational resources provided by the Centre de Supercomputació de Catalunya (CESCA) and the Centro de Supercomputación de Galicia (CESGA: ICTS-2009-40).

References

[1] Laser Interferometer Space Antenna (LISA) URLs: `www.esa.int`, `lisa.jpl.nasa.gov`
[2] Danzmann K 2003 *Advances in Space Research* **32** 1233–1242
[3] Prince T 2003 *American Astronomical Society Meeting* **202** 3701
[4] Finn L S and Thorne K S 2000 *Phys. Rev.* **D62** 124021 (*Preprint* `gr-qc/0007074`)
[5] Schutz B F 2009 *Class. Quant. Grav.* **26** 094020
[6] Sopuerta C F 2010 *Gravitational Wave Notes* **4**(4) 3–47 (*Preprint* `1009.1402`)
[7] Babak S, Gair J R, Petiteau A and Sesana A 2010 (*Preprint* `1011.2062`)
[8] Amaro-Seoane P *et al.* 2007 *Class. Quant. Grav.* **24** R113–R169 (*Preprint* `astro-ph/0703495`)
[9] Canizares P and Sopuerta C F 2009 *J. Phys. Conf. Ser.* **154** 012053 (*Preprint* `0811.0294`)
[10] Canizares P and Sopuerta C F 2009 *Phys. Rev.* **D79** 084020 (*Preprint* `0903.0505`)
[11] Canizares P, Sopuerta C F and Jaramillo J L 2010 *Phys. Rev.* **D82** 044023 (*Preprint* `1006.3201`)
[12] Thornburg J 2010 (*Preprint* `1006.3788`)
[13] Poisson E 2004 *Living Rev. Relativity* **7** 6 (*Preprint* `gr-qc/0306052`) URL `http://www.livingreviews.org/lrr-2004-6`
[14] Barack L 2009 *Class. Quant. Grav.* **26** 213001 (*Preprint* `0908.1664`)
[15] Barack L and Ori A 2000 *Phys. Rev.* **D61** 061502 (*Preprint* `gr-qc/9912010`)
[16] Barack L 2000 *Phys. Rev.* **D62** 084027 (*Preprint* `gr-qc/0005042`)
[17] Barack L 2001 *Phys. Rev.* **D64** 084021 (*Preprint* `gr-qc/0105040`)
[18] Barack L, Mino Y, Nakano H, Ori A and Sasaki M 2002 *Phys. Rev. Lett.* **88** 091101 (*Preprint* `gr-qc/0111001`)
[19] Mino Y, Nakano H and Sasaki M 2002 *Prog. Theor. Phys.* **108** 1039–1064 (*Preprint* `gr-qc/0111074`)
[20] Barack L and Ori A 2002 *Phys. Rev.* **D66** 084022 (*Preprint* `gr-qc/0204093`)
[21] Detweiler S, Messaritaki E and Whiting B F 2003 *Phys. Rev.* **D67** 104016 (*Preprint* `gr-qc/0205079`)
[22] Haas R and Poisson E 2006 *Phys. Rev.* **D74** 044009 (*Preprint* `gr-qc/0605077`)
[23] Sopuerta C F and Laguna P 2006 *Phys. Rev.* **D73** 044028 (*Preprint* `gr-qc/0512028`)
[24] Boyd J P 2001 *Chebyshev and Fourier Spectral Methods* 2nd ed (New York: Dover)
[25] Diaz-Rivera L M, Messaritaki E, Whiting B F and Detweiler S 2004 *Phys. Rev.* **D70** 124018 (*Preprint* `gr-qc/0410011`)
[26] Lau S R 2004 *Class. Quant. Grav.* **21** 4147–4192
[27] Zenginoglu A 2010 *ArXiv e-prints* (*Preprint* `1008.3809`)